Cancer Cell
Article

HRG Inhibits Tumor Growth and Metastasis by Inducing Macrophage Polarization and Vessel Normalization through Downregulation of PlGF

Charlotte Rolny,[1,2,3,10] Massimiliano Mazzone,[2,3,10] Sònia Tugues,[1] Damya Laoui,[4,5] Irja Johansson,[1] Cathy Coulon,[2,3] Mario Leonardo Squadrito,[6] Inmaculada Segura,[2,3] Xiujuan Li,[1] Ellen Knevels,[2,3] Sandra Costa,[2,3] Stefan Vinckier,[2,3] Tom Dresselaer,[7] Peter Åkerud,[8] Maria De Mol,[2,3] Henriikka Salomäki,[1] Mia Phillipson,[9] Sabine Wyns,[2,3] Erik Larsson,[1] Ian Buysschaert,[2,3] Johan Botling,[1] Uwe Himmelreich,[7] Jo A. Van Ginderachter,[4,5] Michele De Palma,[6] Mieke Dewerchin,[2,3] Lena Claesson-Welsh,[1,11,*] and Peter Carmeliet[2,3,11]
[1]Uppsala University, Department of Genetics and Pathology, Rudbeck Laboratory, 75185 Uppsala, Sweden
[2]Vesalius Research Center, VIB, Leuven, Belgium
[3]Vesalius Research Center, K.U.Leuven, Leuven, Belgium
[4]Laboratory of Cellular Molecular Immunology, Department Molecular Cellular Interactions, VIB, Brussels, Belgium
[5]Laboratory of Cellular Molecular Immunology, Vrije Universiteit Brussel, Brussels, Belgium
[6]Angiogenesis & Tumor Targeting Unit, HSR-TIGET, and Vita-Salute University, San Raffaele Scientific Institute, 20132 Milan, Italy
[7]MoSAIC, K.U. Leuven, Belgium
[8]Uppsala University, Department Surgical Sciences, University Hospital, 75185 Uppsala
[9]Uppsala University, Department Medical Cell Biology, Biomedical Center, Uppsala, Sweden
[10]These authors contributed equally to this work
[11]These authors contributed equally to this work
*Correspondence: lena.welsh@igp.uu.se
DOI 10.1016/j.ccr.2010.11.009

SUMMARY

Polarization of tumor-associated macrophages (TAMs) to a proangiogenic/immune-suppressive (M2-like) phenotype and abnormal, hypoperfused vessels are hallmarks of malignancy, but their molecular basis and interrelationship remains enigmatic. We report that the host-produced histidine-rich glycoprotein (HRG) inhibits tumor growth and metastasis, while improving chemotherapy. By skewing TAM polarization away from the M2- to a tumor-inhibiting M1-like phenotype, HRG promotes antitumor immune responses and vessel normalization, effects known to decrease tumor growth and metastasis and to enhance chemotherapy. Skewing of TAM polarization by HRG relies substantially on downregulation of placental growth factor (PlGF). Besides unveiling an important role for TAM polarization in tumor vessel abnormalization, and its regulation by HRG/PlGF, these findings offer therapeutic opportunities for anticancer and antiangiogenic treatment.

INTRODUCTION

Angiogenesis and inflammation are hallmarks of cancer. Tumor vessels are irregular, disorderly structured, and inefficiently perfused, thereby impairing perfusion and drug delivery (Jain, 2005). The resulting hypoxia creates a hostile milieu from where cancer cells escape through a leaky endothelium (Mazzone et al., 2009). Traditional antiangiogenic "vessel pruning" agents can aggravate tumor hypoxia and worsen malignancy (Bergers and Hanahan, 2008). Antiangiogenic "vessel normalizing" strategies are gaining attention, as they can silence metastasis and improve anticancer therapies. However, the basis of vessel abnormalization remains enigmatic.

Infiltration of tumor-associated macrophages (TAMs) is associated with an unfavorable prognosis (Qian and Pollard, 2010). However, not only their numbers but also their phenotype

Significance

M2-like TAMs promote malignancy by suppressing antitumor immune responses and stimulating angiogenesis. Also, since tumor vessels function poorly, tumor perfusion, oxygenation, and chemotherapy are impaired, while enhancing metastasis. Traditional antiangiogenic "vessel pruning" strategies can worsen this situation by aggravating hypoxia. Our findings are significant as (1) they unveil an important role of TAM polarization in vessel abnormalization; (2) they imply that reeducation of TAM polarization is a promising anticancer treatment strategy; (3) they identify HRG as an anticancer drug target, that combats malignancy by enhancing immunity and vessel normalization; (4) they stress the potential of antiangiogenic "vessel normalizing" strategies in silencing metastasis; and (5) they provide support for PlGF-blockage for treatment of cancer.

regulates tumorigenesis. In nonprogressing or regressing tumors, TAMs are biased to a classic macrophage activation M1-like program, characterized by proinflammatory activity, antigen presentation and tumor lysis. In malignant tumors, TAMs resemble alternatively activated macrophages (M2-type), that increase angiogenesis and tumor cell intra/extravasation and growth; they suppress antitumor immunity by preventing activation of dendritic cells (DCs), cytotoxic T lymphocytes (CTLs), and natural killer (NK) cells (Mantovani and Sica, 2010; Qian and Pollard, 2010). It is unknown if TAMs regulate tumor vessel abnormalization.

TAMs consist of distinct subsets (Mantovani and Sica, 2010; Qian and Pollard, 2010), which coexist in tumors, adapt to the changing milieu, and can be re-educated by immunoregulatory cues (Movahedi et al., 2010; Pucci et al., 2009). This has primed interest in developing therapies, aimed at skewing TAMs to an M1-like phenotype (De Palma et al., 2008). Nonetheless, only few molecules have been identified to orchestrate this process so far.

In this study, we explored if histidine-rich glycoprotein (HRG), a host-produced antiangiogenic and immunomodulatory factor, regulates tumor vessel abnormalization and inflammation, for various reasons. First, HRG is a multidomain protein that binds thrombospondins (TSPs), heparin, FcγR receptors and other molecules, implicated in tumorigenesis (Blank and Shoenfeld, 2008; Jones et al., 2005). Second, HRG is deposited in the tumor stroma from plasma or platelets (Klenotic et al., 2010; Thulin et al., 2009), but tumor HRG levels have been only analyzed in a few human cancers (Klenotic et al., 2010; Simantov et al., 2001). Third, binding of HRG to its ligands is facilitated by Zn^{2+} and low pH, conditions found in the tumor milieu. Fourth, HRG stimulates phagocytosis of dying cells (Poon et al., 2010a), but it is unknown if it regulates TAM polarization. Fifth, HRG inhibits tumor growth (Dixelius et al., 2006; Karrlander et al., 2009; Olsson et al., 2004), but its precise mechanisms remain incompletely understood. Moreover, a role for HRG in metastasis has not been documented yet.

HRG's antitumor activity has been ascribed to effects on tumor vessels, but these reports are not unequivocal. Indeed, by inhibiting antiangiogenic agents, HRG may stimulate angiogenesis (Klenotic et al., 2010; Simantov et al., 2001). On the other hand, HRG inhibits endothelial cell (EC) responses. It blocks binding of FGFs to heparan sulfate, prevents release of angiogenic factors from the matrix (Jones et al., 2004; Poon et al., 2010b), and inhibits growth factor-induced EC migration (Dixelius et al., 2006). Binding of HRG to tropomyosin has also been proposed to underly its antiangiogenic activity (Guan et al., 2004). In tumors, HRG counteracts PDGF-driven angiogenesis (Karrlander et al., 2009), while HRG deficiency increases angiogenesis (Thulin et al., 2009). Nonetheless, it has not been established if these in vitro mechanisms underlie the in vivo antiangiogenic effects of HRG in tumors. This is a relevant question, as HRG affects other cell types, such as macrophages, known to regulate angiogenesis. Whether HRG regulates tumor angiogenesis indirectly through TAMs has not been explored.

The goal of this study was to identify mechanisms mediating the antitumor effects of HRG, with focus on its previously documented immune modulatory function (Blank and Shoenfeld, 2008), and to reveal molecular links between HRG and regulators of pathological angiogenesis.

RESULTS

Expression of HRG in Human Cancer

We immunostained samples from 20 healthy and malignant human tissues. HRG was prominent in healthy liver and less abundant around vessels, macrophages, and other cell types in healthy tissues (Figure 1A). Consistent with reports that HRG binds to cell surfaces (Hulett and Parish, 2000), a HRG immunoreactive signal was detected on other cell types. This signal was weaker in malignant than healthy cells (especially in hepatocellular carcinoma cells) and weaker in stromal cells of tumors compared to healthy tissues (Figure 1B; see Figures S1A–S1D and Table S1 available online). Only in brain tumors was the HRG signal somewhat stronger than in healthy brain, consistent with another report (Klenotic et al., 2010), likely because plasma HRG leaked through the disrupted blood-brain barrier (Figure S1D). Overall, HRG levels are decreased in human cancer.

Genetic Gain-of-Function Strategy to Study the Role of HRG in Tumors

To study the role of HRG in cancer, we used a gain-of-function approach to overcome the decreased tumor HRG levels. Reasoning that overexpression of HRG by tumor cells would result in stromal deposition, we transduced T241 fibrosarcoma, Panc02 pancreatic tumor and 4T1 breast tumor lines with a lentiviral vector, encoding human HRG ($hHRG^+$) and GFP; control cells were transduced with a vector expressing only GFP (Ctrl). GFP expression was controlled by an internal ribosomal entry site and therefore not detected by direct fluorescence, neither on HRG^+ nor on Ctrl tumor sections. None of the HRG^+ tumor lines expressed mouse HRG (not shown), but produced hHRG in vitro (HRG^+ T241 tumor: 991 ng/10^7 cells/24 hr) (Figure 1C).

hHRG was deposited in HRG^+ but not in control T241 tumors grown in mice (Figures 1D and 1E). When tumors grew to larger sizes, the HRG^+ signal became weaker (Figures S1E–S1G), while plasma levels of human HRG decreased (from ~100 μg/ml at day 14 to ~5 μg/ml at day 21). Since GFP remained detectable by anti-GFP antibodies, it raised the question whether HRG became degraded by tumor cell-produced proteases; HRG is indeed partially degraded to inactive fragments by tumors (not shown). To avoid any confounding interpretation due to degradation of HRG, tumor studies were performed during the window of HRG expression. RT-PCR showed that murine HRG was undetectable in cancer-associated fibroblasts (CAFs), TAMs and tumor ECs (tECs), sorted from intact tumors (not shown).

HRG Inhibits Tumor Growth and Metastasis

When implanted in wild-type (WT) mice, HRG^+ tumors grew slower and metastasized less. HRG reduced the growth of subcutaneous T241 fibrosarcomas, orthotopic Panc02 pancreatic tumors and 4T1 breast tumors by 62%, 26%, and 36%, respectively (Figures 1F–1I). HRG also decreased Panc02 lymph node metastasis by 62% (Figure 1J) and 4T1 lung metastasis by 90% (Figure 1K). As HRG decreased the metastatic index (nodules per gram tumor), the reduced tumor spread was partly independent of tumor growth inhibition. Since metastatic nodule formation was reduced, but lodging to the lung was unaffected (Figure S1H), the decreased metastasis is attributable to reduced escape from the primary tumor. However, delayed

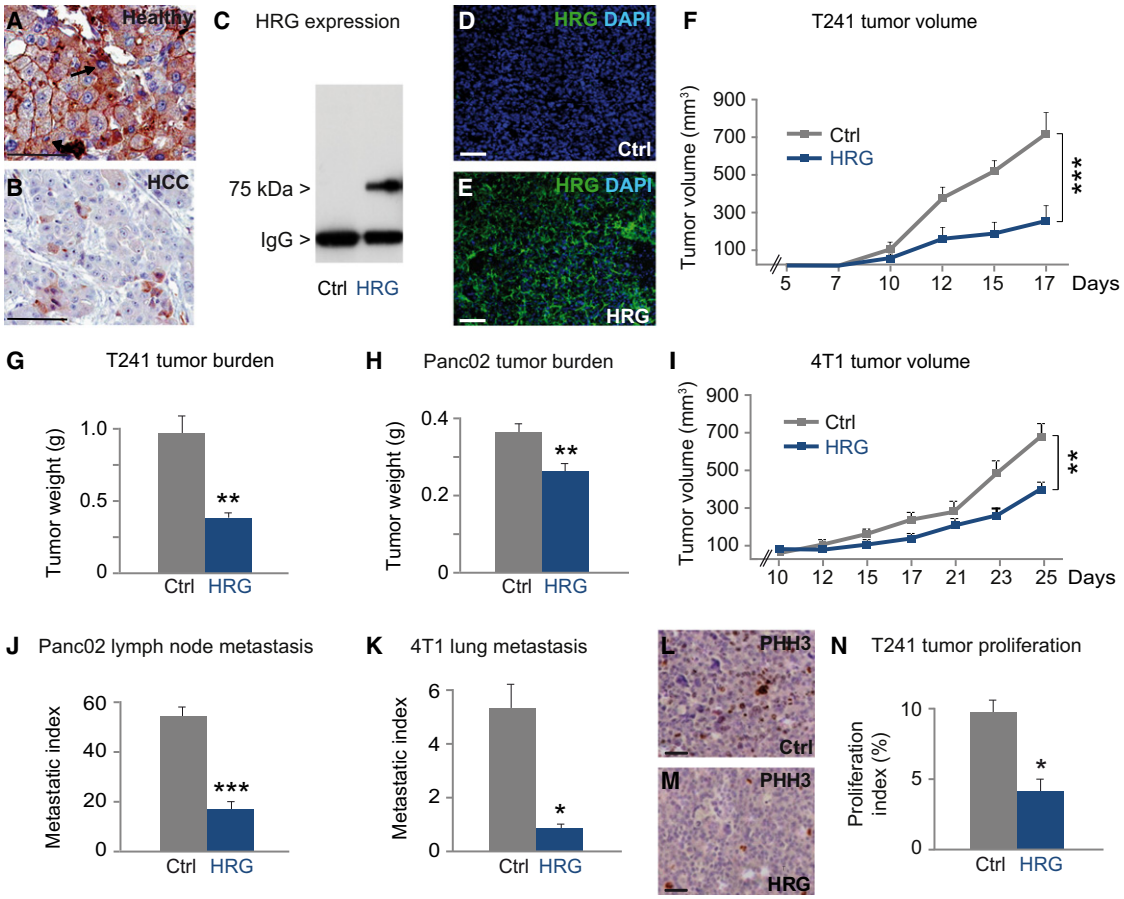

Figure 1. Reduction of Tumor Growth by HRG

(A and B) HRG immunostaining, showing stronger HRG$^+$ signal in healthy liver than in hepatocytocellular carcinoma (HCC). Bars: 20 μm.

(C) Production of HRG by HRG$^+$ but not control (Ctrl) T241 cells.

(D and E) HRG immunostaining (green) of T241 tumors, showing expression of HRG in HRG$^+$ (E) but not control (D) tumors. Bars: 50 μm.

(F and G) T241 model, showing slower growth of HRG$^+$ tumors (F; n = 13; ***$p < 0.001$); similar findings for end-stage tumor weight (G; n = 20; **$p < 0.01$).

(H and I) Panc02 (H; n = 13; **$p < 0.01$) and 4T1 (I; n = 8; **$p < 0.01$) model, showing slower growth of HRG$^+$ tumors.

(J and K) Reduced metastasis of HRG$^+$ tumors in Panc02 model (J; n = 13; ***$p < 0.001$; lymph node metastasis) and 4T1 model (K; n = 8; *$p < 0.05$; pulmonary metastasis).

(L–N) PHH3 staining, revealing fewer proliferating tumor cells in HGR$^+$ (M) than control (L) T241 tumors; (N) proliferation index (PHH3$^+$/total cells) (n = 5; *$p < 0.05$). Bars: 20 μm.

Data represent mean ± SEM; statistical significance was assessed by t test. See also Figure S1.

growth of HRG$^+$ metastases also contributed to the decreased metastatic burden (Figure S1I). Staining for phosphohistone-H3 showed that proliferation was reduced in HRG$^+$ T241 tumors (Figures 1L–1N). As HRG$^+$ tumor cell proliferation was normal in vitro (Figure S1J), stromal rather than tumor cell autonomous mechanisms accounted for the decreased tumor cell proliferation in vivo. We thus focused on vessel normalization and antitumor immunity, known to regulate tumor growth and metastasis (Mantovani and Sica, 2010; Mazzone et al., 2009).

HRG Promotes Vessel Normalization and Improves Tumor Perfusion

We first studied angiogenesis in HRG$^+$ tumors, not only because the reduced growth of HRG$^+$ tumors might be caused by blockage of angiogenesis, but also because the decreased metastasis of HRG$^+$ tumors might be due to "normalization" of tumor vessels. Staining for the EC marker CD31 showed that vessel density and average vessel area were comparable in control and HRG$^+$ T241 tumors (Figures 2A–2D). When analyzing the distribution of vessel size, we observed a shift toward smaller vessels (Figure S2A). Since these parameters do not necessarily correlate with vessel function, we studied perfusion by delivery of FITC-conjugated lectin. Nearly double the number of vessels was perfused in HRG$^+$ T241 tumors (Figures 2E–2G). HRG$^+$ tumors were less hypoxic, as assessed by pimonidazole (PIMO) staining at early (12 days) and late stage (19 days) (Figures 2H–2J), and displayed smaller necrotic and hemorrhagic areas (Figures 2K–2N). MRI confirmed that HRG$^+$ tumors were less necrotic (Figures S2B and S2C). HRG$^+$ tumors were also less apoptotic (Figures 2O–2Q). Since pericyte coverage improves vessel maturation, we double stained for CD31 and the pericyte marker α-smooth muscle actin (αSMA) and

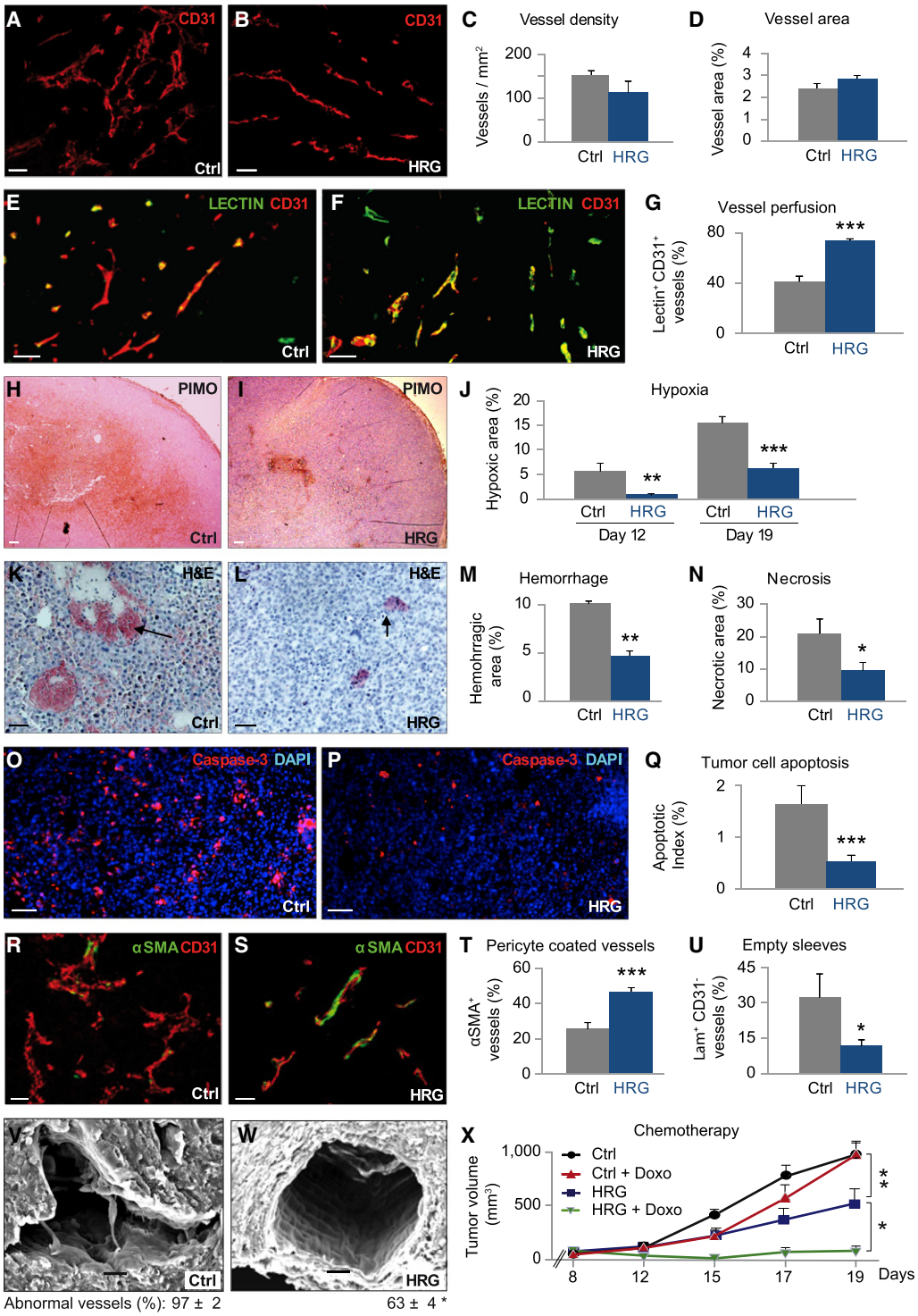

Figure 2. HRG Improves Tumor Vessel Maturation and Normalization

(A–D) Staining for CD31 (red) in control (A) and HRG$^+$ (B) T241 tumors. (C and D) Vessel density (C) and area (D; CD31$^+$ area, %).

(E–G) Staining for FITC-conjugated lectin (green) and CD31 (red) in control (E) and HRG$^+$ (F) T241 tumors. (G) Increase in perfused lectin$^+$CD31$^+$ vessels (% of CD31$^+$ vessels) in HGR$^+$ tumors (n = 6; ***p < 0.001).

(H–J) Staining for pimonidazole (PIMO; brown), revealing smaller hypoxic regions in HRG$^+$ (I) than control (H) tumors. Morphometry (J) revealed reduced PIMO$^+$ area (% of tumor area) in HRG$^+$ T241 tumors (n = 8; **p < 0.01; ***p < 0.001).

(K–N) H&E staining, showing less hemorrhaging (M; arrows) and necrosis (N) in HRG$^+$ (L) than control (K) T241 tumors. (M and N) Analysis of necrotic and hemorrhagic area (% of tumor area) (n = 7; *p < 0.05, **p < 0.01).

observed an increased pericyte coverage of tumor vessels in HRG$^+$ tumors (Figures 2R–2T); similar numbers of PDGFRα^+ cancer-associated fibroblast/myofibroblasts (CAFs) were present (not shown). HRG$^+$ tumor edema was also reduced ([wet-dry weight]/dry weight, ×100: 80 ± 2 for controls versus 73 ± 2 for HRG$^+$; n = 5; p = 0.06).

Further characterization of the tumor vasculature in orthotopic Panc02 tumors confirmed that HRG promoted vessel normalization. HRG$^+$ tumors contained fewer "empty sleeves," i.e., channels with a laminin$^+$ basement membrane devoid of CD31$^+$ ECs (Figure 2U). HRG also improved the stability and tightness of the EC layer, since the junctional molecule VE-cadherin was continuous over longer distances and more abundant in HRG$^+$ tumor vessels (Figures S2D–S2G). Scanning electron microscopy (SEM) showed that fewer vessels in HRG$^+$ Panc02 tumors contained abnormal multilayers of disconnected ECs with multiple protrusions (Figures 2V and 2W). Administration of the cytotoxic agent doxorubicin at a suboptimal dose (2.5 mg/kg, 3×/wk) was ineffective in reducing growth of control T241 tumors, but decreased HRG$^+$ T241 tumor growth by 50% (Figure 2X). Overall, HRG improved tumor vessel maturation and perfusion, reduced hypoxia and improved chemotherapy. Also, the tighter EC barrier is known to reduce metastasis (Mazzone et al., 2009). The improved tumor vessel normalization and maturation could thus explain the antimetastatic activity of HRG.

Effects of HRG on Tumor-Associated Macrophage Polarization

Since the vascular changes alone unlikely explained the inhibition of tumor growth by HRG, we explored if HRG affected the immune response. We focused on TAMs, as their accumulation correlates with tumor progression. However, F4/80$^+$ TAM accumulation was only slightly increased in HRG$^+$ T241 tumors (Figures 3A–3C), and comparable in HRG$^+$ Panc02 (see below) and 4T1 (not shown) models. HRG$^+$ T241 tumors had comparable numbers of myeloid cells (CD11b$^+$ cells, percentage of viable cells: 15 ± 3 for control versus 20 ± 1 for HRG$^+$; n = 3; p = 0.18) or contained slightly more CD11b$^+$ F4/80$^+$ macrophages (12 ± 2 for control versus 16 ± 0.2 for HRG$^+$; n = 3; p = 0.01). Levels of *Ccl2* (also known as *Mcp1*), *Csf2* (*Gm-csf*), and *Csf1* (*M-csf*), i.e., chemotactic cytokines for macrophages, were not altered in HRG$^+$ tumors (Figures S3A–S3C). Overall, HRG only caused insignificant changes in the extent of myeloid cell infiltration.

Because tumor growth was reduced despite persistent TAM accumulation, we analyzed the phenotype of freshly isolated TAMs. Protumoral and proangiogenic (i.e., M2-like) TAMs express elevated levels of the mannose receptor-1 (MRC1), arginase-1 (Arg1), IL-10 and the chemokines CCL22 and CCL17 (Movahedi et al., 2010; Pucci et al., 2009). Conversely, antitumoral and proinflammatory (i.e., M1-like) TAMs express higher levels of inflammatory and antiangiogenic cytokines such as IL-1, IL-6, Type I interferons (IFNs), IL-12, and CXCL9 (Mantovani et al., 2002). TNFα marks M1- and M2-oriented TAMs (Hagemann et al., 2008; Movahedi et al., 2010; Qian and Pollard, 2010). We found that 2-fold fewer F4/80$^+$ TAMs expressed MRC1 in HRG$^+$ T241 tumors (Figures 3A, 3B, and 3D). F4/80$^+$ TAMs from HRG$^+$ tumors expressed reduced levels of other M2-type genes (Figures 3E and 3F), as well as of TNFα (pg/ml: 141 in control versus 72 in HRG$^+$) and IL-10 (64 pg/ml for control versus 24 pg/ml in HRG$^+$).

Conversely, F4/80$^+$ TAMs from HRG$^+$ T241 tumors upregulated the M1-type genes *Cxcl9* (Figure 3F), *IFN-β* (mRNA copies/10^4 *Hprt* mRNA copies: 2.7 ± 0.02 for control versus 8.7 ± 2.0 for HRG$^+$; n = 4; p = 0.04) and IL-6 (pg/ml: 182 in control versus 644 in HRG$^+$). Expression of *IL-12* also tended to be upregulated (mRNA copies/10^3 *Hprt* mRNA copies: 3.7 ± 0.6 for control versus 24 ± 16 for HRG$^+$; n = 5; p = 0.10). Although IL-1β is regarded as an M1 marker, it also has angiogenic and metastatic activity (Arteta et al., 2010); in line with the antiabnormalization/metastatic effects of HRG, *IL-1β* levels were reduced in TAMs from HRG$^+$ tumors (Figure 3G). Similar findings, including downregulation of *Ccl17*, were obtained when analyzing F4/80$^+$CD11c$^+$ cells (Figures S3D–S3F), which mostly comprise M1-type TAMs (Movahedi et al., 2010; Pucci et al., 2009). Overall, HRG skewed TAM polarization away from the M2-like phenotype.

Mechanistic analysis revealed that HRG skewed TAM polarization via direct effects, as exposure of peritoneal macrophages (pMØs) to HRG upregulated *Cxcl9* and *IFN-β* and downregulated expression of *Ccl22* and *IL-10* (Figures S3G–S3J). However, the M1-skewed TAM polarization in response to HRG was not attributable to an increase in circulating inflammatory (CD115$^+$CD11b$^+$Gr1^{high}) over "resident" (CD115$^+$CD11b$^+$Gr1^{low}) monocytes (Figure S3K). Also, the lower number of MRC1$^+$ TAMs in HRG$^+$ T241 tumors was not due to apoptosis of this population, as shown by comparable numbers of TUNEL$^+$ or 7AAD$^+$ MRC1$^+$F4/80$^+$ cells upon immunostaining of tumor sections or flow cytometry of TAMs, respectively (Figure S3L; not shown).

Additional Effects of HRG on Tumor Immunity

HRG also promoted the host-antitumor immune response by affecting dendritic cells (DCs). Indeed, HRG$^+$ tumors contained more CD11c$^+$ cells (Figures 3H–3J; Figure S3M), the majority

(O–Q) Staining for cleaved caspase-3 (red) revealed fewer apoptotic cells in HRG$^+$ (P) than control (O) T241 tumors; (Q) apoptotic index (caspase-3$^+$ / total cells) (n = 6; ***p < 0.01).

(R–T) Double staining for CD31 (red) and α-SMA (green), showing more pericyte-covered tumor vessels in HRG$^+$ (S) than control (R) tumors, quantified in (T) (α-SMA$^+$CD31$^+$ vessels, percentage of CD31$^+$ vessels; n = 6; ***p < 0.001).

(U) Counting of vessels, stained for laminin and CD31, showing fewer "empty sleeves" in HRG$^+$ Panc02 tumors (n = 5; *p < 0.05).

(V and W) SEM micrographs, showing abnormal tumor vessel containing multilayers of disconnected ECs with luminal protrusions in control tumor (V) and normalized vessel, lined by monolayer of cobblestone ECs in a HRG$^+$ Panc02 tumor (W). Numbers below panels indicate fraction of abnormal vessels (% of vessels analyzed) (n = 5; *p < 0.0.5).

(X) Doxorubicine (Doxo) treatment of T241 tumor-bearing mice, showing that a suboptimal dose did not affect growth of control tumors (Ctrl), but inhibited growth of HRG$^+$ T241 tumor growth (n = 6; *p < 0.05). In the absence of doxorubicin, HRG$^+$ tumor growth was significantly suppressed compared to control (n=6; **p < 0.01). Bars in all tissue section panels: 10 μm.

Data represent mean ± SEM; statistical significance was assessed by t test. See also Figure S2.

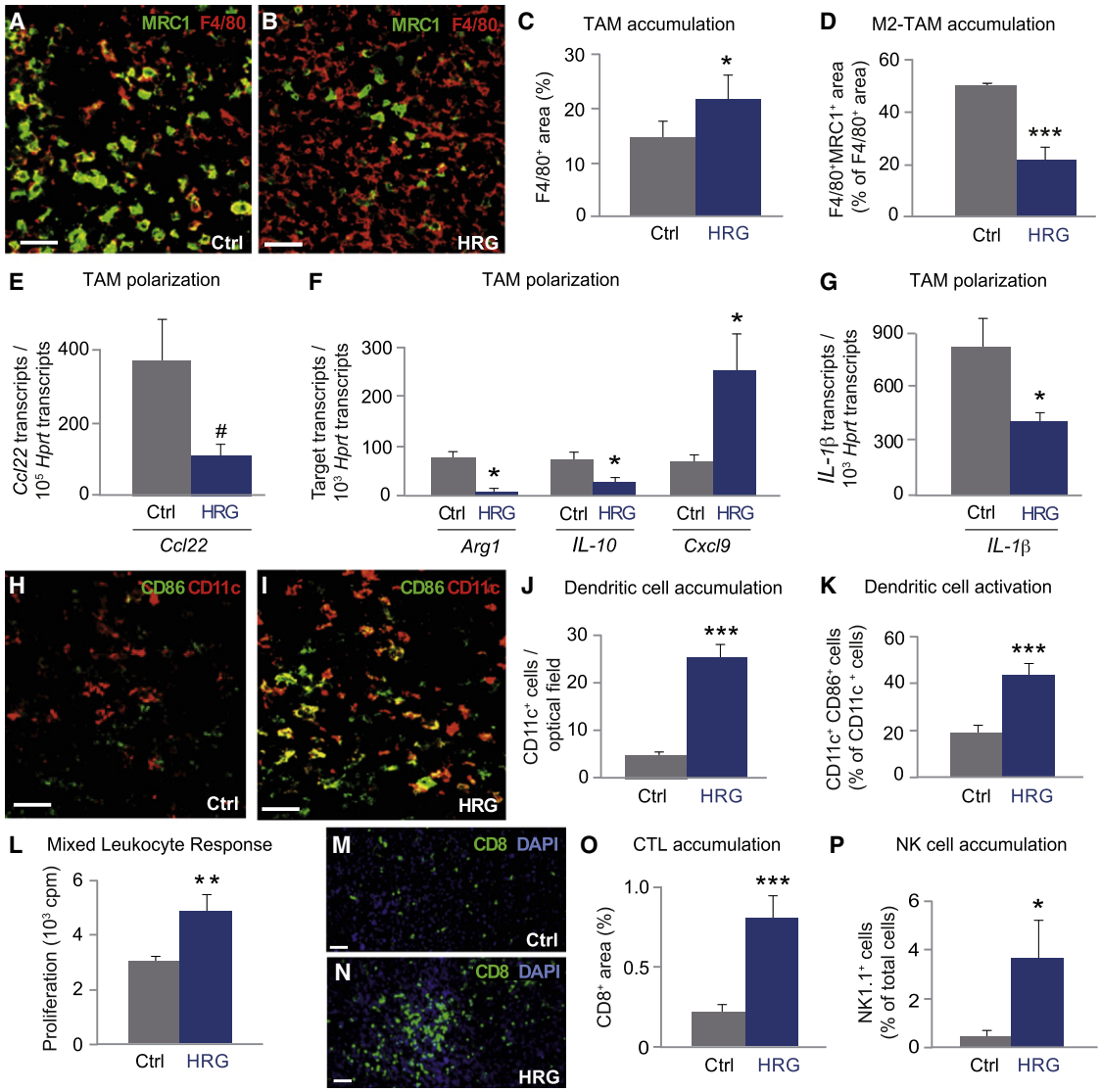

Figure 3. Effects of HRG on TAM Polarization

(A–D) Double staining for F4/80 (red) and MRC1 (green), revealing slightly more F4/80$^+$ macrophages but fewer F4/80$^+$MRC1$^+$ macrophages in HRG$^+$ (B) than control (A) T241 tumors. (C) quantification of F4/80$^+$ area (% of tumor area) (n = 5; *p < 0.05); (D) quantification of the F4/80$^+$MRC1$^+$ area (% of F4/80$^+$ tumor area) (n = 6; **p < 0.01). Bars: 20 μm.

(E–G) RT-PCR, revealing that FACS-sorted macrophages from HRG$^+$ T241 tumors expressed reduced levels of *Ccl22* (E), *IL-10* and *Arg1* (F) and *IL-1β* (G), while expressing increased levels of *Cxcl9* (F) (n = 5–12; *p < 0.05 and #p = 0.068).

(H–K) Double staining for CD11c (red) and CD86 (green), revealing more CD11c$^+$ cells in HRG$^+$ (I) than control (H) T241 tumors. (J) Quantification of CD11c$^+$ cells per optical field (n = 5; ***p < 0.01). (K) Higher percentage of CD11c$^+$CD86$^+$ cells (% of CD11c$^+$ cells; n = 5; ***p < 0.01) in HRG$^+$ tumors. Bars: 20 μm.

(L) Mixed leukocyte response (MLR) assay, showing higher induction of CD8$^+$ T cell proliferation by Cd11c$^+$F4/80$^+$ TAMs from HRG$^+$ than Ctrl T241 tumors.

(M–O) Staining for CD8 (green), revealing more cytotoxic CD8$^+$ T cells in HRG$^+$ (N) than control (M) T241 tumors; (O) quantification of CD8$^+$ area (% of tumor area) (n = 7; ***p < 0.001). CTL, cytotoxic T cell lymphocytes. Bars: 20 μm.

(P) Flow-cytometry, showing more NK1.1$^+$ natural killer (NK) cells in HRG$^+$ than control T241 tumors (n = 6; *p < 0.05). Cells were gated as viable (7AAD$^-$) CD45^{+-} CD11b$^-$NK1.1$^+$ cells and quantified in percent of total cells after physical gating.

Data represent mean ± SEM; statistical significance was assessed by t test. See also Figure S3.

of which coexpressed CD86 (Figures 3H, 3I, and 3K; Figure S3N) and MHC class II (CD11c$^+$MHC class II$^+$, percentage of CD11b$^+$ cells: 1.3 ± 0.5 in control versus 14.6 ± 1.7 in HRG$^+$; n = 6; p < 0.001), suggesting that they are activated DCs, though their molecular signature overlaps with M1-polarized TAMs (Pucci et al., 2009). Also, antigen-presenting cells from HRG$^+$ T241 tumors stimulated allogeneic CD8$^+$ T cell proliferation more than corresponding cells from control tumors (Figure 3L). HRG stimulated DC activation indirectly, since it did not affect or only marginally influenced the expression of the DC maturation markers MHC class II, CD83, or CD86 (not shown).

HRG$^+$ T241 tumors also contained higher numbers of CD8$^+$ cytotoxic T lymphocytes (CTLs) (Figures 3M–3O; Figure S3O) and NK1.1$^+$ NK cells (Figure 3P), while CD4$^+$ T cells were not

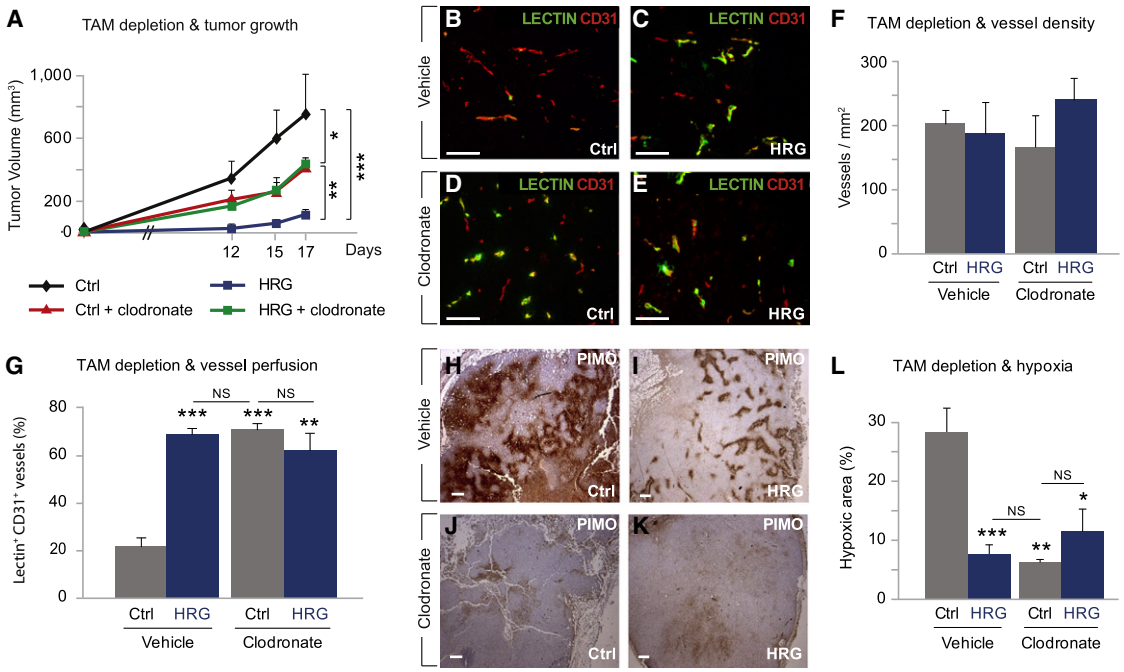

Figure 4. Effects of Macrophage Depletion on the Effects of HRG

(A) Treatment with clodronate reduced control 4T1 tumor growth and enhanced HRG$^+$ tumor growth (relative to vehicle liposome controls). Similar effects in T241 tumors (not shown) (n = 10; $p < 0.001$, 2-way ANOVA; $^{**}p < 0.01$, $^{***}p < 0.001$ versus control, Bonferroni post hoc test).

(B–G) Staining for CD31 (red) and lectin (green), revealing perfused CD31$^+$lectin$^+$ vessels and nonperfused CD31$^+$lectin$^-$ vessels in control (B and D) and HRG$^+$ (C and E) T241 tumors in mice, treated with vehicle (B and C) or clodronate (D and E) liposomes. (F) Quantification of CD31$^+$ vessels revealed comparable density in control and HRG$^+$ tumors in mice receiving vehicle or clodronate liposomes. (G) Quantification of CD31$^+$lectin$^+$ vessels (% of CD31$^+$ vessels) revealed a larger fraction of perfused vessels in HRG$^+$ tumors in mice receiving vehicle liposomes. In clodronate-treated mice, the fraction of perfused vessels was increased comparably in control and HRG$^+$ tumors. (F and G) n = 5; $^{**}p < 0.01$ and $^{***}p < 0.001$ versus Ctrl vehicle. Bars: 50 μm.

(H–L) Immunostaining for pimonidazole (PIMO; brown), revealing PIMO$^+$ hypoxic areas in control (H and J) and HRG$^+$ (I,K) T241 tumors in mice, treated with vehicle (H and I) or clodronate (J and K) liposomes. (L) Quantification of PIMO$^+$ area (percentage of tumor area) revealed smaller hypoxic regions in HRG$^+$ tumors in mice receiving vehicle liposomes. In clodronate-treated mice, hypoxic tumor regions were decreased comparably in control and HRG$^+$ tumors. (L) n = 5; $^*p < 0.05$, $^{**}p < 0.01$ and $^{***}p < 0.001$ versus Ctrl vehicle. Bars: 100 μm.

Data represent mean ± SEM; statistical significance was assessed by t test, or as indicated. See also Figure S4.

affected (not shown). Immunodepletion of CTLs and NK cells showed that HRG increased their lytic activity for tumor cells. Indeed, when administering anti-CD8 antibodies, depletion of CTLs tended to increase the growth of control tumors by 1.6-fold ($p = 0.07$) as compared with CTL-complete control tumors, treated with control IgG (Figure S3P). In contrast, CTL depletion enhanced the growth of HRG$^+$ T241 tumors by up to 5-fold ($p = 0.01$; Figure S3P). Analogous studies with anti-NK1.1 antibodies revealed that NK-depleted HRG$^+$ tumors grew 7-fold faster than NK-complete HRG$^+$ tumors treated with control IgG (Figure S3P). Although HRG itself did not affect T cell proliferation (not shown), TAMs from HRG$^+$ tumors upregulated IL-6, IL-12, and IFN-β, which are known activators of T cells and NK cells, suggesting that HRG induced CTLs/immune responses indirectly via skewing of TAM polarization. Overall, HRG promoted a Th1/M1-skewed antitumor immune response, known to inhibit tumor growth.

TAM Depletion Abrogates the Effects of HRG in Cancer

To underscore that TAM polarization inhibited tumor growth, metastasis, and vessel abnormalization, we treated tumor-bearing mice with clodronate liposomes to chemically deplete TAMs (using vehicle liposomes as control), and compared its effects in control tumors (containing more M2-skewed TAMs) with HRG$^+$ tumors (containing more M1-skewed TAMs). Elimination of TAMs decreased the growth of control tumors, indicating that TAMs were predominantly of the M2-like, tumor-promoting phenotype in these conditions. Vehicle liposome-treated HRG$^+$ T241 tumors were smaller, but depletion of TAMs by clodronate liposomes enhanced their growth (Figure 4A), showing that HRG skewed TAMs to a more tumor-inhibitory M1-like phenotype. Clodronate also reduced dissemination of control tumors (Figure S4), indicating that TAMs exerted a prometastatic activity, in accordance with their M2-like phenotype. Metastasis of vehicle liposome-treated HRG$^+$ tumors was reduced, but TAM depletion did not further affect metastasis (Figure S4), indicating that M1-polarized TAMs in HRG$^+$ T241 tumors did not (prominently) regulate this process.

We also examined if TAMs participated in tumor vessel abnormalization, and if such a role was related to their M1/M2-like phenotype. In control tumors, clodronate improved tumor perfusion (Figures 4B, 4D, and 4G) and oxygenation (Figures 4H, 4J, and 4L). Perfusion and oxygenation were improved in vehicle liposome-treated HRG$^+$ tumors, but TAM depletion failed

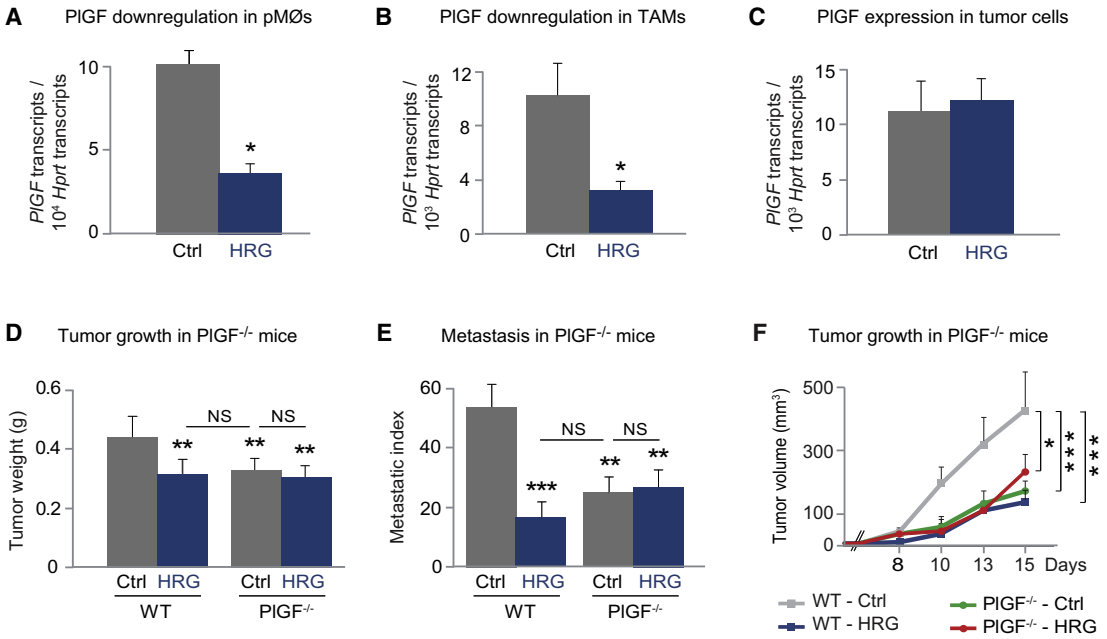

Figure 5. Role of PlGF in the Antitumor/Metastatic Activity of HRG

(A–C) RT-PCR, showing reduced *Plgf* transcript levels in pMØs treated with HRG (n = 4; $^{**}p < 0.01$) (A), and in F4/80$^+$ TAMs from HRG$^+$ T241 tumors (n = 8–12; $^*p < 0.05$) (B), but not in GFP$^+$ tumor cells (n = 8–12) (C).

(D and E) Analysis of tumor growth (D) and metastatic index (E) in Panc02 tumor model, revealing reduced growth and metastasis of HRG$^+$ tumors in WT mice; growth and metastasis of control and HRG$^+$ tumors was reduced comparably in PlGF$^{-/-}$ mice (n = 17; $^{**}p < 0.01$ versus control tumors in WT mice). Data in (D) and (E) represent mean ± SEM; statistical significance was assessed by t test.

(F) Similar findings were observed in the T241 tumor model (n = 7, $^*p < 0.05$, $^{***}p < 0.001$ by 2-way ANOVA). See also Figure S5.

to further affect these parameters (Figures 4C, 4E, 4G, 4I, 4K, and 4L), showing that M1-polarized TAMs did not (prominently) regulate tumor vessel abnormalization. No effects on vessel density were observed in either condition (Figure 4F). Thus, the antivessel abnormalization activity of HRG relied on its ability to skew TAM polarization away from the M2-like provessel abnormalization phenotype.

HRG Downregulates the Expression of PlGF by TAMs

We then searched for a possible downstream target of HRG that mediates TAM polarization, and analyzed the expression of candidate genes by treating pMØs with HRG. HRG decreased the expression of *Plgf* (Figure 5A), but not of other angiogenic regulators (Figure S5A). This downregulation was also observed in TAMs, freshly isolated from HRG$^+$ T241 tumors (Figure 5B), but it was cell type specific, as HRG failed to alter *Plgf* levels in ECs, CAFs, or tumor cells (Figure 5C; not shown). Not unexpectedly, the profile of other genes, such as *Vegf* and *Pdgfb*, in pMØs treated with HRG differed from that in TAMs from HRG$^+$ tumors, as the latter sensed not only the direct effect of HRG but also the indirect environmental changes induced by HRG (Figure S5B).

Role of PlGF in the Antitumor/Antimetastatic Activity of HRG

To investigate if downregulation of TAM-derived PlGF mediated the antitumor activity of HRG, we compared control and HRG$^+$ Panc02 tumor cells in WT and PlGF-deficient (PlGF$^{-/-}$) mice. In WT mice, growth of HRG$^+$ tumors was impaired (Figure 5D). Growth of control tumors was slower in PlGF$^{-/-}$ mice (Figure 5D), in accordance with findings that stromal PlGF promotes tumor growth (Carmeliet et al., 2001). However, in PlGF$^{-/-}$ mice, growth of HRG$^+$ and control Panc02 tumors was reduced to the same extent (Figure 5D), indicating that HRG did not further suppress tumor growth in the absence of host-derived PlGF. Similar observations were made when analyzing metastasis (Figure 5E). Use of the T241 tumor model confirmed that growth of control and HRG$^+$ tumors was comparably reduced in PlGF$^{-/-}$ mice (Figure 5F). Thus, HRG inhibited tumor growth and metastasis, but only if stromal cells expressed PlGF.

To explore if a myeloid cell type in the tumor stroma was the responsible PlGF producer, we examined if PlGF in bone marrow-derived myeloid cells (BMCs) was required for the antitumor activity of HRG and therefore transplanted PlGF$^{-/-}$ bone marrow in irradiated WT hosts (KO→WT) and, as control, WT bone marrow in WT recipients (WT→WT). Compared with WT→WT mice, growth and metastasis of control Panc0 tumors were reduced in KO→WT mice (Figures S5C–S5E) to the same extent as for HRG$^+$ tumors in WT→WT mice or in KO→WT mice. Thus, HRG overexpression phenocopied the BMC-specific loss of PlGF, and HRG could not further affect tumor growth and spreading in the absence of BMC-produced PlGF, indicating that HRG blocked tumorigenesis via downregulation of TAM-produced PlGF.

Role of PlGF in TAM Polarization by HRG

We then investigated if PlGF mediated HRG's effects on TAM polarization. Confirming the lack of an effect by HRG on TAM infiltration, F4/80$^+$ TAM accumulation was comparable in control

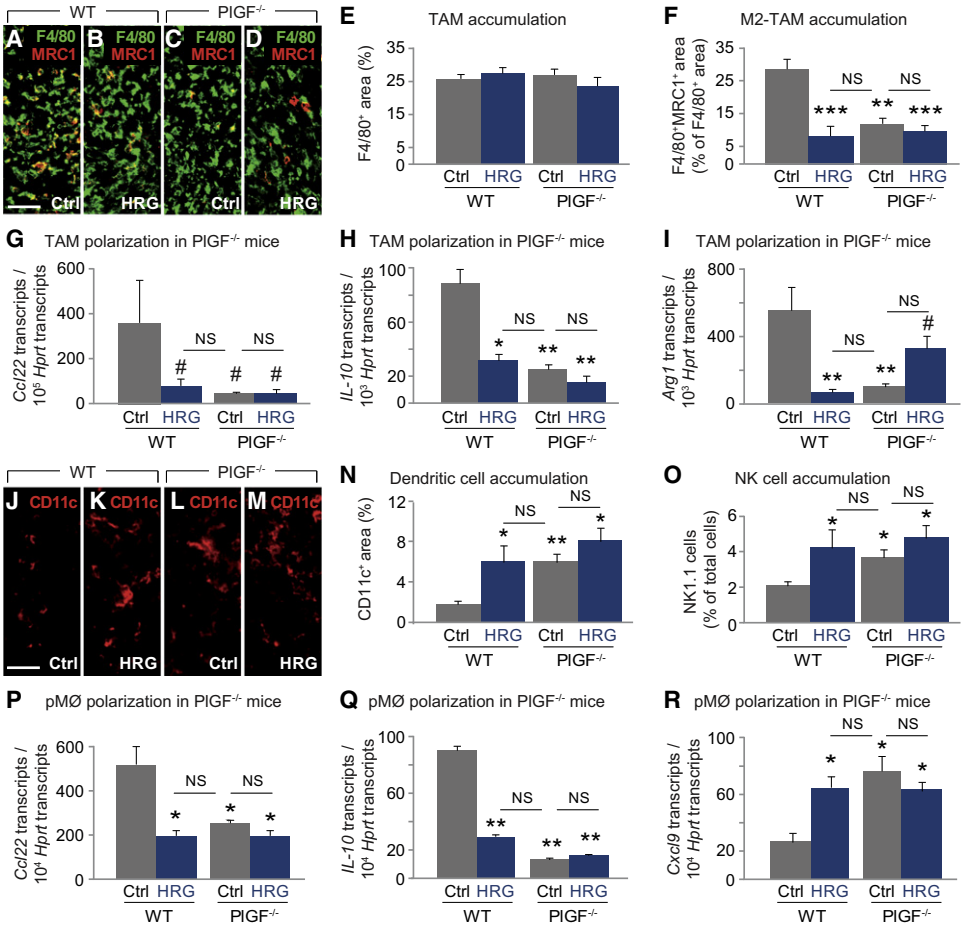

Figure 6. HRG Attenuates the Proangiogenic M2 Gene Profile

(A-F) Staining of Panc02 tumors for F4/80 (green) and MRC1 (red), revealing MRC1$^+$/F4/80$^+$ (yellow) macrophages in control (A and C) and HRG$^+$ (B and D) tumors in WT (A and B) and PlGF$^{-/-}$ (C and D) mice. (E and F) Quantification revealed similar F4/80$^+$ TAM accumulation (E; F4/80$^+$ area, percentage of tumor) in each condition, but fewer MRC1$^+$/F4/80$^+$ TAMs in HRG$^+$ tumors in WT mice (F); infiltration of MRC1$^+$/F4/80$^+$ TAMs was comparably reduced in control and HRG$^+$ tumors in PlGF$^{-/-}$ mice (F; n = 5; **p < 0.01 and ***p < 0.001 versus control tumors in WT mice). Bars: 20 μm.

(G–I) RT-PCR, showing lower expression of *Ccl22* (G), *IL-10* (H), and *Arg1* (I) in flow-sorted F4/80$^+$ TAMs from HRG$^+$ than control (Ctrl) T241 tumors in WT mice; expression of these genes was comparably decreased in control and HRG$^+$ tumors in PlGF$^{-/-}$ mice (n = 5–10; $^{\#}$p = 0.07; *p < 0.05; **p < 0.01, versus control tumors in WT mice).

(J–N) Staining of Panc02 tumors for CD11c (red), revealing dendritic cells in control (J and L) and HRG$^+$ (K and M) tumors in WT (J and K) and PlGF$^{-/-}$ (L and M) mice. (N) Quantification revealed more CD11c$^+$ cells (CD11c$^+$ area, percentage of tumor area) in HRG$^+$ tumors in WT mice; infiltration of CD11c$^+$ cells was comparably increased in control and HRG$^+$ tumors in PlGF$^{-/-}$ mice (N; n = 5; *p < 0.05, **p < 0.01 versus control tumors in WT mice). Bars: 20 μm.

(O) Flow sorting of NK1.1$^+$ cells, revealing larger fraction of NK cells in HRG$^+$ T241 tumors in WT mice; infiltration of NK1.1$^+$ cells was comparably increased in control and HRG$^+$ tumors in PlGF$^{-/-}$ mice (n = 6; *p < 0.05).

(P and Q) RT-PCR, showing reduced expression of *Ccl22* (P) and *IL-10* (Q) in HRG-treated WT pMØs; expression was comparably reduced in Ctrl or HRG-treated PlGF$^{-/-}$ pMØs (n = 3–6; *p < 0.05, **p < 0.01 versus control WT).

(R) RT-PCR, showing upregulation of *Cxcl9* in HRG-treated WT pMØs; expression of *Cxcl9* was comparably increased in control or HRG-treated PlGF$^{-/-}$ pMOs (n = 4; **p < 0.01 versus control WT).

Data represent mean ± SEM; statistical significance was assessed by t test.

and HRG$^+$ tumors in PlGF$^{-/-}$ mice (Figures 6A, 6C, and 6E). In contrast, loss of stromal PlGF affected TAM polarization. In control tumors, MRC1 was expressed in fewer F4/80$^+$ TAMs in PlGF$^{-/-}$ mice (Figures 6A, 6C, and 6F), but the number of F4/80$^+$MRC1$^+$ TAMs was reduced to the same extent in control and HRG$^+$ tumors in PlGF$^{-/-}$ mice (Figures 6B, 6D, and 6F). F4/80$^+$ TAMs, sorted from control tumors in PlGF$^{-/-}$ mice or HRG$^+$ tumors in WT mice, expressed lower levels of the M2 genes *Ccl22*, *IL-10*, and *Arg1*; this profile was not further altered in HRG$^+$ Panc02 tumors in PlGF$^{-/-}$ mice (Figures 6G–6I). Similar findings were obtained when analyzing F4/80$^+$CD11c$^+$ cells (Figures S3D–S3F). In accordance with findings that the increased infiltration of DCs and NK cells in HRG$^+$ T241 tumors in WT mice resulted from TAM polarization, more of these cells infiltrated control tumors in PlGF$^{-/-}$ mice (Figures 6J, 6L, 6N, and 6O), showing that PlGF deficiency altered tumor immunity. However, HRG overexpression did not further affect the infiltration of these cells in PlGF$^{-/-}$ mice (Figures 6K, 6M–6O).

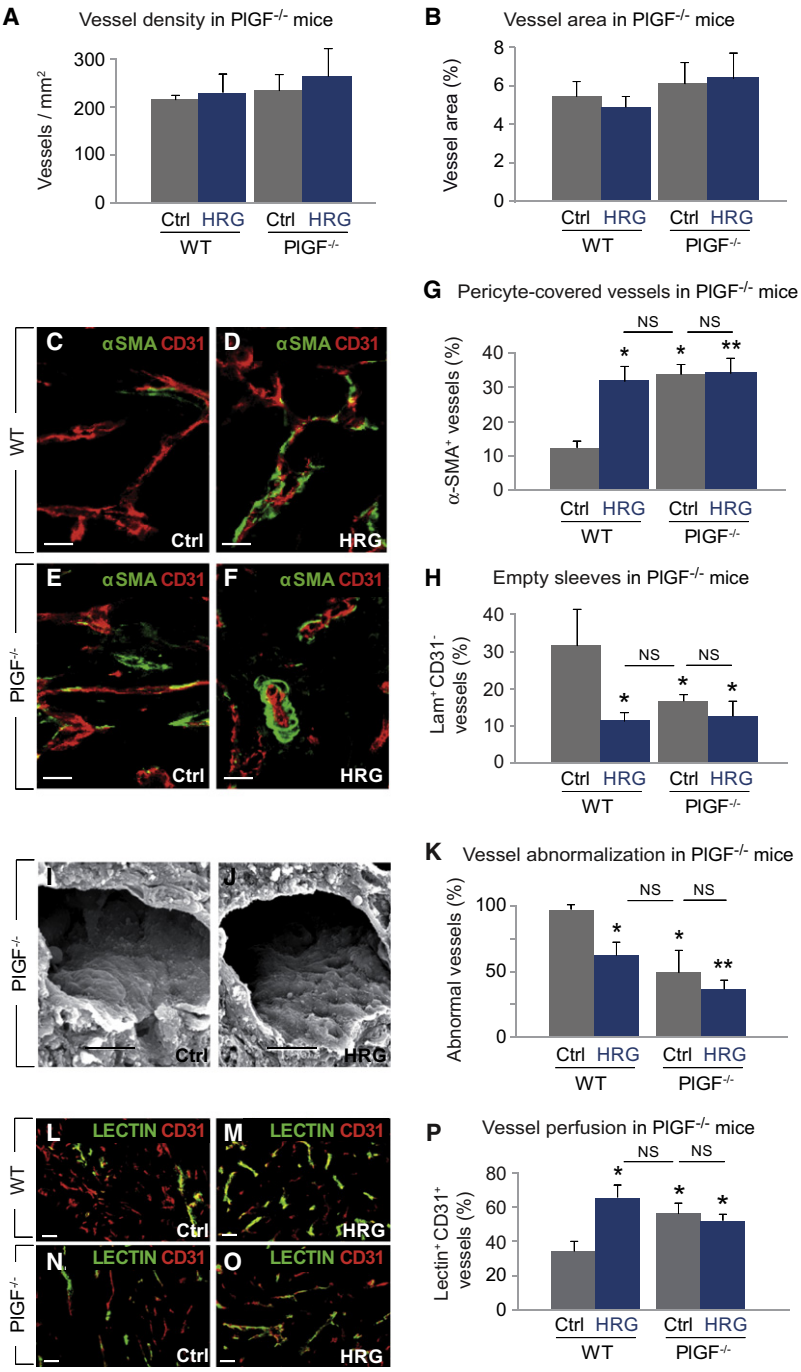

Figure 7. Improved Tumor Vessel Maturation and Normalization in PlGF$^{-/-}$ Mice

(A and B) Immunostaining for CD31, revealing similar vessel density (A) and area (B; CD31$^+$ area, percentage of tumor area) in control and HRG$^+$ Panc02 tumors in WT or PlGF$^{-/-}$ mice (n = 5).

(C–G) Double staining for CD31 (red) and α-SMA (green), revealing pericyte-coated CD31$^+$αSMA$^+$ vessels in control (C and E) and HRG$^+$ (D and F) tumors in WT (C and D) and PlGF$^{-/-}$ (E and F) mice. (G) Quantification revealed more CD31$^+$αSMA$^+$ vessels (percentage of CD31$^+$ vessels) in HRG$^+$ tumors in WT mice; the fraction of CD31$^+$αSMA$^+$ vessels was comparably increased in control and HRG$^+$ Panc02 tumors in PlGF$^{-/-}$ mice (n = 7; *p < 0.05, **p < 0.01 versus control tumor in WT).

(H) Counting of vessels, double stained for laminin and CD31 showed fewer "empty sleeves" (laminin$^+$ structures devoid of a CD31$^+$ EC lining) in HRG$^+$ tumors in WT mice; the fraction of empty sleeves was comparably decreased in control and HRG$^+$ Panc02 tumors in PlGF$^{-/-}$ mice (laminin$^+$CD31$^-$ vessels, percentage of laminin$^+$ vessels; n = 5; *p < 0.05 versus control tumor in WT).

(I–K) SEM micrographs, showing normalized vessel, lined by monolayer of cobblestone-like ECs, in a control (I) and HRG$^+$ (J) Panc02 tumor in PlGF$^{-/-}$ mice. (K) Quantification revealed fewer abnormalized vessels (percentage of vessels analyzed) in HRG$^+$ than control tumors in WT mice; the fraction of abnormalized vessels was comparably decreased in control and HRG$^+$ tumors in PlGF$^{-/-}$ mice (n = 5; *p < 0.05 **p < 0.01 versus control tumors in WT mice).

(L–P) Staining for CD31 (red) and perfusion dye FITC-conjugated lectin (green), revealing perfused CD31$^+$lectin$^+$ vessels and nonperfused CD31$^+$lectin$^-$ vessels in control (L and N) and HRG$^+$ (M and O) Panc02 tumors in WT (L and M) and PlGF$^{-/-}$ (N and O) mice. (P) Quantification showed more CD31$^+$lectin$^+$ vessels (percentage of CD31$^+$ vessels) in HRG$^+$ tumors in WT mice; the fraction of CD31$^+$lectin$^+$ vessels was comparably increased in control and HRG$^+$ tumors in PlGF$^{-/-}$ mice (n = 5; *p < 0.05 versus control tumors in WT mice).

Data represent mean ± SEM; statistical significance was assessed by t test. Bars: 10 μm in C–F, I, J; 50 μm in L–O. See also Figure S6.

We also assessed if autocrine production of PlGF by TAMs controlled their polarization. PlGF$^{-/-}$ pMØs expressed lower levels of *Ccl22* and *IL-10* (Figures 6P and 6Q; Figures S3I and S3J), but higher levels of *Cxcl9* and *IFN-β* (Figure 6R; Figures S3G and S3H). Moreover, WT pMØs treated with anti-PlGF antibodies displayed a similar M1-skewed profile as PlGF$^{-/-}$ pMØs (Figures S3G–S3J). HRG did not further affect the expression of M2- or M1-specific genes in PlGF$^{-/-}$ pMØs or in WT pMØs treated with anti-PlGF (Figures 6P–6R; Figures S3G–S3J). Overall, genetic loss or pharmacologic blockage of PlGF as well as downregulation of PlGF by HRG skewed polarization of pMØs/TAMs away from the M2-like phenotype.

Role of PlGF in HRG-Mediated Vessel Normalization

We also explored if PlGF downregulation acted downstream of HRG in regulating vessel normalization. Vessel density and average size were comparable in WT and PlGF$^{-/-}$ mice, both for control and HRG$^+$ Panc02 tumors (Figures 7A and 7B). Also, the same changes in the distribution of vessel area detected in HRG$^+$ tumors in WT mice were observed both in control and HRG$^+$ tumors in PlGF$^{-/-}$ mice (Figure S2A). Blocking stromal- or tumor-produced PlGF inhibits tumor angiogenesis and TAM accumulation (Fischer et al., 2007; Van de Veire et al., 2010); however, the normal vessel density and infiltration of TAMs in the absence of stromal PlGF

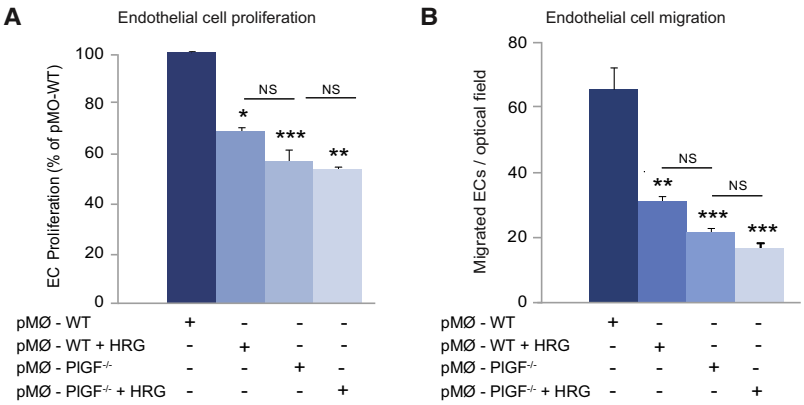

Figure 8. Macrophage Polarization by HRG Inhibits EC Responses

(A) ECs were stimulated in vitro with medium, conditioned by vehicle- or HRG-treated WT pMØs (pMØ-WT and pMØ-WT+HRG, respectively), or by vehicle- or HRG-treated PlGF$^{-/-}$ pMØ (pMØ-PlGF$^{-/-}$ or pMØ-PlGF$^{-/-}$+HRG, respectively). EC proliferation was only minimally affected by HRG directly (not shown), but inhibited by medium conditioned by pMØ-WT+HRG, pMØ-PlGF$^{-/-}$, and pMØ-PlGF$^{-/-}$+HRG. y axis: number of ECs, percentage of ECs stimulated with medium conditioned by pMO-WT (n = 4; *p < 0.05, **p < 0.01, ***p < 0.001).

(B) Similar results were obtained when analyzing direct and indirect effects of HRG on EC migration. y axis: number of ECs per optical field (OF) (n = 3; **p < 0.01 ***p < 0.001).

Data represent mean ± SEM; statistical significance was assessed by t test. See also Figure S7.

were likely rescued by production of PlGF (or other factors) by tumor cells (Coenegrachts et al., 2010); also, angiogenesis and TAM infiltration in certain tumor models are PlGF independent (Van de Veire et al., 2010).

However, other parameters of vessel function in control tumors were affected by stromal loss of PlGF, similar as in HRG^{+} Panc02 tumors in WT mice. Indeed, in control tumors in PlGF$^{-/-}$ mice, vessel maturation was improved, while vessel remodeling was reduced (Figures 7C, 7E, 7G, and 7H). Similar changes were observed in HRG^{+} Panc02 tumors in PlGF$^{-/-}$ mice, indicating that HRG was unable to further regulate these processes in the absence of stromal PlGF (Figures 7C–7H). Also, SEM revealed that the fraction of vessels, lined by an abnormal EC layer, was comparably decreased in control and HRG^{+} Panc02 tumors in PlGF$^{-/-}$ mice, to the same extent as in HRG^{+} tumors in WT mice (Figures 7I–7K; see Figures 2V and 2W for comparison). Similar findings were made when analyzing the number of perfused vessels (Figures 7L–7P) and the tightness of the EC barrier (Figure S6).

Bone marrow transplantation studies revealed that PlGF in BMCs was the target of HRG's activity to improve vessel perfusion. Indeed, the decrease in hypoxia in HRG^{+} tumors in WT→WT mice also occurred in control tumors in KO→WT mice, while hypoxia was not further decreased in HRG^{+} tumors in KO→WT mice (Figure S7). Thus, loss of stromal BMC-derived PlGF phenocopied the effects of HRG overexpression in WT mice, but HRG did not further affect these processes in PlGF$^{-/-}$ or KO→WT mice, suggesting that PlGF acted downstream of HRG in regulating vessel abnormalization.

Finally, in vitro experiments established that HRG affected ECs indirectly via TAM polarization in a PlGF-dependent manner. Indeed, HRG did not affect EC proliferation or migration, while these responses were reduced by conditioned medium from HRG-treated WT pMØs and from PlGF$^{-/-}$ pMØs (Figures 8A and 8B) or from anti-PlGF-treated WT pMØs (all M1 skewed; not shown). EC migration and proliferation were not further reduced by HRG treatment of PlGF$^{-/-}$ pMØs (Figures 8A and 8B). Overall, HRG induced vessel normalization primarily via indirect effects through TAM polarization, rather than via direct effects on ECs, and PlGF acted downstream of HRG in this process.

DISCUSSION

Here, we report that HRG, a host-produced protein deposited in the tumor stroma, combats tumor progression and dissemination by enforcing the anticancer immune response and promoting tumor vessel normalization, respectively. Critically underlying these activities is the ability of HRG to skew TAM polarization away from their proangiogenic /immune-suppressive M2-like phenotype.

HRG Induces Changes in TAM Phenotypes

Macrophage depletion showed that TAMs mediated the antitumor effects of HRG. While not affecting infiltration, HRG skewed TAM phenotypes. Indeed, depletion of TAMs decreased progression of control tumors, while increasing growth of HRG^{+} tumors, implying that TAMs acquired a tumor-suppressive M1-like phenotype when exposed to HRG. Expression profiling and immunophenotyping confirmed TAM skewing by HRG, while in vitro experiments showed that HRG affected polarization via direct effects. In the tumor milieu, HRG might also influence TAM polarization indirectly via effects on oxygenation. Since hypoxia stimulates M2-like polarization (Lewis et al., 2007), improved oxygenation in HRG^{+} tumors can provide a self-reinforcing stimulus for further polarizing TAMs away from an M2-like phenotype.

Rather than reprogramming TAMs to an "M1-only" profile in an all-or-none fashion, HRG induced a "HRG-specific" polarization signature. Indeed, HRG downregulated established M2 markers (Arg1, IL-10, MCR1, CCL17, CCL22), but also induced changes in gene expression, that at first sight may appear more atypical. For instance, HRG reduced the expression of TNFα and IL-1β, cytokines with a proinflammatory activity. However, M1-TAMs may express reduced levels of TNFα (Hagemann et al., 2008; Movahedi et al., 2010) and IL-1β (Mantovani and Sica, 2010), in line with our findings. Moreover, since IL-1β promotes angiogenesis and metastasis (Arteta et al., 2010), its reduced levels in HRG^{+} tumors could contribute to the decreased metastasis and enhanced vessel normalization. Overall, the HRG-induced polarization signature endowed TAMs with an ability to inhibit tumor (vessel) growth and metastasis.

HRG Improves Tumor Vessel Normalization

Untreatable metastasis is often the cause of mortality in cancer patients. A prominent environmental stimulus of tumor dissemination is hypoxia, resulting from poorly functioning abnormalized tumor vessels. Our findings suggest that HRG inhibited metastasis in part by altering vessel morphology. These changes, ranging from an increased pericyte coverage, tightened EC barrier and smoother EC layer, promoted vessel normalization, perfusion, and oxygenation. Hence, by creating a less hypoxic milieu, HRG diminished the need for tumor cells to escape. In addition, by tightening the EC layer, HRG likely created a more impenetrable barrier for tumor cells to intravasate and spread to distant tissues.

A noteworthy finding was that the changes in vessel function were accompanied by subtle changes in vessel numbers, possibly because vessel branching is more sensitive to changes in TAM accumulation, which was not affected by HRG. Nonetheless, the clodronate studies indicate that depletion of the predominantly M2-skewed TAMs from control tumors normalized the tumor vasculature, while elimination of the mainly M1-skewed TAMs from HRG^+ tumors was ineffective. This suggests that M2-like TAMs induce vessel abnormalization, while M1-like TAMs are not/less involved. Although TAMs promote tumor angiogenesis (De Palma et al., 2007; Qian and Pollard, 2010), we here link TAM polarization to vessel abnormalization. We speculate that M2-polarized TAMs render vessels abnormal by expressing increased amounts or different sets of angiogenic factors. Also, upregulation of angiogenic M2-cytokines (IL-10, CCL22, IL-1β, TNFα) or downregulation of angiostatic M1-cytokines (IFN-β, CXCL10, IL-12) could contribute to vessel abnormalization. Though HRG can counteract vessel abnormalization via direct effects on ECs as well as indirectly via effects on TAM polarization, the finding that depletion of TAMs abrogated the vascular effects of HRG suggest that the indirect effects of HRG via TAM polarization are likely predominant in the tumor microenvironment in situ.

HRG Promotes Tumor Immunity

HRG also increased the host-antitumor immune response. Indeed, HRG not only increased tumor infiltration by antigen presenting DCs, cytolytic NK cells and cytotoxic T-lymphocytes, but also enhanced their antigen presentation and tumor cell lysis potential, immune changes known to inhibit tumor growth (Mantovani and Sica, 2010). Even though HRG binds to T cells and stimulates their adhesion in vitro, it is unknown if these changes activate T cells. Since HRG did not affect T cell proliferation in vitro (not shown), HRG likely promoted immunity indirectly via effects on TAM polarization. The observed shift in cytokine/chemokine profile is consistent herewith. Indeed, TAMs from HRG^+ tumors expressed lower levels of IL-10, known to inhibit the potential of DCs and macrophages to activate T cells (Koppelman et al., 1997), while producing higher levels of IL-6, IL-12, and IFN-β, known to stimulate T cell proliferation and activation of DCs and NK cells (DeNardo et al., 2010; Mantovani and Sica, 2010). HRG may further enforce the antitumor response by improving perfusion and thereby tumor influx of immune effector cells (Hamzah et al., 2008). Moreover, by facilitating clearance of dying tumor cells (Blank and Shoenfeld, 2008), HRG could further contribute to tumor shrinkage. Thus, by enhancing not only the effector performance but also the influx of immune cells, HRG fuels the host-antitumor response.

HRG and PlGF: A Molecular Link

That PlGF downregulation by HRG is relevant was evidenced by in vitro and in vivo experiments. First, loss of PlGF phenocopied the inhibitory effects of HRG on tumor growth, metastasis, and vessel abnormalization. Second, conditioned medium of $PlGF^{-/-}$ macrophages or anti-PlGF-treated WT macrophages phenocopied HRG's effects on EC responses. Third, loss or inhibition of PlGF in macrophages phenocopied the effect of HRG on TAM polarization. Fourth, HRG was ineffective in the absence of PlGF in the in vitro and in vivo experiments. However, while these studies identified PlGF downregulation as a downstream mechanism of HRG, HRG might also engage additional pathways given its multidomain structure and binding characteristics. Genetic and pharmacological studies implicated PlGF in angiogenesis and inflammation in pathological conditions (Fischer et al., 2008; Van de Veire et al., 2010). In contrast, Hedlund and coworkers reported that overexpression of PlGF in tumor cells promotes tumor vessel normalization (Hedlund et al., 2009). This is, however, only an apparent paradox, as overexpression of PlGF leads to formation of VEGF/PlGF heterodimers and therefore a reduction in proangiogenic VEGF homodimers. The present findings underscore the dual activity of PlGF on vessels and myeloid cells, but also unveil unknown roles of PlGF on TAM polarization.

Possible Implications

Our findings have a number of implications: (1) it is tempting to speculate that deposition of an antiangiogenic/immunomodulatory molecule like HRG in the tumor stroma is a host defense mechanism against the growing cancer and that HRG participates in the recognition of "malignant danger," in line with its presumed role as a "pattern recognition molecule" (Poon et al., 2010a); the tumor, in turn, may try to escape from this host-attack by downregulating or degrading HRG; (2) our findings unveil a role of M2-TAM polarization in vessel abnormalization and imply that re-education of TAM polarization is a promising anticancer strategy; (3) they further highlight the potential of antiangiogenic "vessel normalizing" strategies in silencing metastasis and stress the importance of analyzing vessel/TAM function rather than their numbers alone; how anti-abnormalization strategies best fit in current antiangiogenic therapy warrants further analysis; finally, (4) the data also provide further support for PlGF-blockage strategies for the treatment of cancer.

EXPERIMENTAL PROCEDURES

More detailed methods can be found in the Supplemental Experimental Procedures.

Animals

C57BL/6 mice and Balb/c (8–12 weeks old) were obtained from VIB mouse facility or from Mollegard/Bomhultgard, Denmark. PlGF-deficient ($PlGF^{-/-}$) mice were described previously (Carmeliet et al., 2001). Housing and experimental animal procedures were approved by the K.U. Leuven Animal Care and Research Advisory Committee and Uppsala University board of animal experimentation.

Tumor Models, Cell Depletion, and BM Transplantation

T241 fibrosarcoma and Panc02 tumor models were described (Mazzone et al., 2009). Tumor volumes were measured with a caliper (length × width^2 × π /6). TAM depletion was achieved by using clodronate as described (Mazzone et al., 2009). CD8$^+$ lymphocytes were depleted by the rat anti-CD8 antibody 53.6.72 (25 mg/kg; Bio X Cell) and NK cells by the mouse anti-NK1.1 antibody PK136 (25 mg/kg; Bio X Cell). T cells purified from Balb/c splenocytes were cultured with C57BL/6 TAMs, and proliferation was measured. Bone marrow from PlGF$^{-/-}$ mice was infused in the tail vein of lethally irradiated WT mice, and 6 weeks later, Panc02 tumor cells were injected orthotopically in the pancreas.

Histology of Human and Mouse Tissues

Tissue microarrays (TMAs) of healthy and malignant tissues, containing multiple samples from different humans with the same diagnosis (432 tumor samples, 20 different cancers) produced by the Human Proteome Atlas (HPA) facility (http://www.proteinatlas.org) were stained using anti-HRG antiserum (#0119) (Dixelius et al., 2006; Kampf and Ostermeyer, 2004; Olsson et al., 2004), and stained TMA sections were scanned by high-resolution scanners (ScanScope XT, Aperio Technologies), separated in individual spot images, and evaluated by experienced pathologists. Ethical permit to use anonymized, decoded (i.e., nontraceable) human fresh-frozen normal or tumor tissue for generation of tissue slides or TMAs was granteed by the Uppsala ethical review board in full agreement with the Swedish Ethical Review Act.

Staining, SEM, and analysis of mouse tissues were as described (Mazzone et al., 2009).

Lentiviral Vectors

Full-length human HRG cDNA was cloned in the FUGIE lentiviral backbone, carrying an internal ribosomal entry site; 10^5 tumor cells were transduced with 10^6 U/ml of the specific lentivirus.

Flow Sorting

Tumors were minced in RPMI medium + 0.1% collagenase I (1 hr; 37°C), passed through a 19 G needle, and filtered and cells were centrifuged (5 min; 1000 rpm). After RBC lysis, cells were centrifuged and washed with PBS, incubated with 10% FCS and with anti-F4/80, CD31, CD45, PDGFRα antibody for 30 min. Tumor cells were sorted as F4/80$^-$/GFP$^+$ cells, TAMs as F4/80$^+$/CD45$^+$ cells, tECs as CD31$^+$/CD45$^-$ cells, CAFs as PDGFRα$^+$ cells. For FACS analysis, collagenase-digested tumor cells were incubated with rat anti-mouse FcγIII/II receptor (CD16/CD32) blocking antibodies (4 μg/ml) to block unspecific binding, labeled with 7-amino-actinomycin D (7-AAD) to stain nonviable cells and then with the proper antibodies.

pMØs

pMØs were extracted by peritoneal lavage, counted, and plated overnight and stimulated with appropriate reagents for 4 or 16 hr.

Protein and mRNA Assays

Protein extraction and immunoblot analysis were described (Olsson et al., 2004); RT-PCR was described (Fischer et al., 2007). For cytokine measurements, ELISAs were performed according to the manufacturer's instructions.

Tumor Hypoxia, Perfusion, Edema, and Necrosis

Tumor hypoxia (pimonidazole staining) and perfusion (FITC-labeled lectin) were analyzed as described (Mazzone et al., 2009). Tumor edema was measured as the wet and dry tumor weight. Tumor necrosis was scored on H&E-stained sections. We also used MRI to evaluate tumor edema and necrosis on viable animals at different time points.

Statistics

Data represent mean ± SEM of representative experiments unless otherwise stated. Statistical significance was calculated by t test unless otherwise stated (Prism v4.0b), considering $p < 0.05$ as statistically significant.

SUPPLEMENTAL INFORMATION

Supplemental Information includes Supplemental Experimental Procedures, seven figures, and one table and can be found with this article online at doi:10.1016/j.ccr.2010.11.009.

ACKNOWLEDGMENTS

This study was supported by the Swedish Cancer Society (3820-B04-09XAC), Swedish Research Council (K2005-32X-12552-08A), and by a Wallenberg Scholar grant to L.C.W.; the Swedish Cancer Society (CAN 2008/980) to C.R.; a European Research Council starting grant to M.D.P.; the Belgian State–Federal Science Policy Office (IUAP06/30); a Fund for Scientific Research Flanders (F.W.O.) grant (G.0651.08); and a Susan G. Komen grant (KG080498), Long-term structural funding–Methusalem funding from the Flemish Government to P.C.

Received: February 13, 2010
Revised: August 12, 2010
Accepted: October 25, 2010
Published online: January 6, 2011

REFERENCES

Arteta, B., Lasuen, N., Lopategi, A., Sveinbjornsson, B., Smedsrod, B., and Vidal-Vanaclocha, F. (2010). Colon carcinoma cell interaction with liver sinusoidal endothelium inhibits organ-specific antitumor immunity through interleukin-1-induced mannose receptor in mice. Hepatology *51*, 2172–2182.

Bergers, G., and Hanahan, D. (2008). Modes of resistance to anti-angiogenic therapy. Nat. Rev. Cancer *8*, 592–603.

Blank, M., and Shoenfeld, Y. (2008). Histidine-rich glycoprotein modulation of immune/autoimmune, vascular, and coagulation systems. Clin. Rev. Allergy Immunol. *34*, 307–312.

Carmeliet, P., Moons, L., Luttun, A., Vincenti, V., Compernolle, V., De Mol, M., Wu, Y., Bono, F., Devy, L., Beck, H., et al. (2001). Synergism between vascular endothelial growth factor and placental growth factor contributes to angiogenesis and plasma extravasation in pathological conditions. Nat. Med. *7*, 575–583.

Coenegrachts, L., Maes, C., Torrekens, S., Van Looveren, R., Mazzone, M., Guise, T.A., Bouillon, R., Stassen, J.M., Carmeliet, P., and Carmeliet, G. (2010). Anti-PlGF reduces bone metastasis by blocking tumor cell engraftment and osteoclast differentiation. Cancer Res. *70*, 6537–6547.

De Palma, M., Murdoch, C., Venneri, M.A., Naldini, L., and Lewis, C.E. (2007). Tie2-expressing monocytes: regulation of tumor angiogenesis and therapeutic implications. Trends Immunol. *28*, 519–524.

De Palma, M., Mazzieri, R., Politi, L.S., Pucci, F., Zonari, E., Sitia, G., Mazzoleni, S., Moi, D., Venneri, M.A., Indraccolo, S., et al. (2008). Tumor-targeted interferon-alpha delivery by Tie2-expressing monocytes inhibits tumor growth and metastasis. Cancer Cell *14*, 299–311.

DeNardo, D.G., Andreu, P., and Coussens, L.M. (2010). Interactions between lymphocytes and myeloid cells regulate pro- versus anti-tumor immunity. Cancer Metastasis Rev. *29*, 309–316.

Dixelius, J., Olsson, A.K., Thulin, A., Lee, C., Johansson, I., and Claesson-Welsh, L. (2006). Minimal active domain and mechanism of action of the angiogenesis inhibitor histidine-rich glycoprotein. Cancer Res. *66*, 2089–2097.

Fischer, C., Jonckx, B., Mazzone, M., Zacchigna, S., Loges, S., Pattarini, L., Chorianopoulos, E., Liesenborghs, L., Koch, M., De Mol, M., et al. (2007). Anti-PlGF inhibits growth of VEGF(R)-inhibitor-resistant tumors without affecting healthy vessels. Cell *131*, 463–475.

Fischer, C., Mazzone, M., Jonckx, B., and Carmeliet, P. (2008). FLT1 and its ligands VEGFB and PlGF: drug targets for anti-angiogenic therapy? Nat. Rev. Cancer *8*, 942–956.

Guan, X., Juarez, J.C., Qi, X., Shipulina, N.V., Shaw, D.E., Morgan, W.T., McCrae, K.R., Mazar, A.P., and Donate, F. (2004). Histidine-proline rich glycoprotein (HPRG) binds and transduces anti-angiogenic signals through cell surface tropomyosin on endothelial cells. Thromb. Haemost. *92*, 403–412.

Hagemann, T., Lawrence, T., McNeish, I., Charles, K.A., Kulbe, H., Thompson, R.G., Robinson, S.C., and Balkwill, F.R. (2008). "Re-educating" tumor-associated macrophages by targeting NF-kappaB. J. Exp. Med. *205*, 1261–1268.

Hamzah, J., Jugold, M., Kiessling, F., Rigby, P., Manzur, M., Marti, H.H., Rabie, T., Kaden, S., Grone, H.J., Hammerling, G.J., et al. (2008). Vascular normalization in Rgs5-deficient tumours promotes immune destruction. Nature *453*, 410–414.

Hedlund, E.M., Hosaka, K., Zhong, Z., Cao, R., and Cao, Y. (2009). Malignant cell-derived PlGF promotes normalization and remodeling of the tumor vasculature. Proc. Natl. Acad. Sci. USA *106*, 17505–17510.

Hulett, M.D., and Parish, C.R. (2000). Murine histidine-rich glycoprotein: cloning, characterization and cellular origin. Immunol. Cell Biol. *78*, 280–287.

Jain, R.K. (2005). Normalization of tumor vasculature: an emerging concept in antiangiogenic therapy. Science *307*, 58–62.

Jones, A.L., Hulett, M.D., and Parish, C.R. (2004). Histidine-rich glycoprotein binds to cell-surface heparan sulfate via its N-terminal domain following Zn2+ chelation. J. Biol. Chem. *279*, 30114–30122.

Jones, A.L., Hulett, M.D., and Parish, C.R. (2005). Histidine-rich glycoprotein: a novel adaptor protein in plasma that modulates the immune, vascular and coagulation systems. Immunol. Cell Biol. *83*, 106–118.

Kampf, G., and Ostermeyer, C. (2004). Influence of applied volume on efficacy of 3-minute surgical reference disinfection method prEN 12791. Appl. Environ. Microbiol. *70*, 7066–7069.

Karrlander, M., Lindberg, N., Olofsson, T., Kastemar, M., Olsson, A.K., and Uhrbom, L. (2009). Histidine-rich glycoprotein can prevent development of mouse experimental glioblastoma. PLoS ONE *4*, e8536.

Klenotic, P.A., Huang, P., Palomo, J., Kaur, B., Van Meir, E.G., Vogelbaum, M.A., Febbraio, M., Gladson, C.L., and Silverstein, R.L. (2010). Histidine-rich glycoprotein modulates the anti-angiogenic effects of vasculostatin. Am. J. Pathol. *176*, 2039–2050.

Koppelman, B., Neefjes, J.J., de Vries, J.E., and de Waal Malefyt, R. (1997). Interleukin-10 down-regulates MHC class II alphabeta peptide complexes at the plasma membrane of monocytes by affecting arrival and recycling. Immunity *7*, 861–871.

Lewis, C.E., De Palma, M., and Naldini, L. (2007). Tie2-expressing monocytes and tumor angiogenesis: regulation by hypoxia and angiopoietin-2. Cancer Res. *67*, 8429–8432.

Mantovani, A., and Sica, A. (2010). Macrophages, innate immunity and cancer: balance, tolerance, and diversity. Curr. Opin. Immunol. *22*, 231–237.

Mantovani, A., Sozzani, S., Locati, M., Allavena, P., and Sica, A. (2002). Macrophage polarization: tumor-associated macrophages as a paradigm for polarized M2 mononuclear phagocytes. Trends Immunol. *23*, 549–555.

Mazzone, M., Dettori, D., Leite de Oliveira, R., Loges, S., Schmidt, T., Jonckx, B., Tian, Y.M., Lanahan, A.A., Pollard, P., Ruiz de Almodovar, C., et al. (2009). Heterozygous deficiency of PHD2 restores tumor oxygenation and inhibits metastasis via endothelial normalization. Cell *136*, 839–851.

Movahedi, K., Laoui, D., Gysemans, C., Baeten, M., Stange, G., Van den Bossche, J., Mack, M., Pipeleers, D., In't Veld, P., De Baetselier, P., and Van Ginderachter, J.A. (2010). Different tumor microenvironments contain functionally distinct subsets of macrophages derived from Ly6C(high) monocytes. Cancer Res. *70*, 5728–5739.

Olsson, A.K., Larsson, H., Dixelius, J., Johansson, I., Lee, C., Oellig, C., Bjork, I., and Claesson-Welsh, L. (2004). A fragment of histidine-rich glycoprotein is a potent inhibitor of tumor vascularization. Cancer Res. *64*, 599–605.

Poon, I.K., Hulett, M.D., and Parish, C.R. (2010a). Histidine-rich glycoprotein is a novel plasma pattern recognition molecule that recruits IgG to facilitate necrotic cell clearance via FcgammaRI on phagocytes. Blood *115*, 2473–2482.

Poon, I.K., Parish, C.R., and Hulett, M.D. (2010b). Histidine-rich glycoprotein functions cooperatively with cell surface heparan sulfate on phagocytes to promote necrotic cell uptake. J. Leukoc. Biol. *88*, 559–569.

Pucci, F., Venneri, M.A., Biziato, D., Nonis, A., Moi, D., Sica, A., Di Serio, C., Naldini, L., and De Palma, M. (2009). A distinguishing gene signature shared by tumor-infiltrating Tie2-expressing monocytes, blood "resident" monocytes and embryonic macrophages suggests common functions and developmental relationships. Blood *114*, 901–914.

Qian, B.Z., and Pollard, J.W. (2010). Macrophage diversity enhances tumor progression and metastasis. Cell *141*, 39–51.

Simantov, R., Febbraio, M., Crombie, R., Asch, A.S., Nachman, R.L., and Silverstein, R.L. (2001). Histidine-rich glycoprotein inhibits the antiangiogenic effect of thrombospondin-1. J. Clin. Invest. *107*, 45–52.

Thulin, A., Ringvall, M., Dimberg, A., Karehed, K., Vaisanen, T., Vaisanen, M.R., Hamad, O., Wang, J., Bjerkvig, R., Nilsson, B., et al. (2009). Activated platelets provide a functional microenvironment for the antiangiogenic fragment of histidine-rich glycoprotein. Mol. Cancer Res. *7*, 1792–1802.

Van de Veire, S., Stalmans, I., Heindryckx, F., Oura, H., Tijeras-Raballand, A., Schmidt, T., Loges, S., Albrecht, I., Jonckx, B., Vinckier, S., et al. (2010). Further pharmacological and genetic evidence for the efficacy of PlGF inhibition in cancer and eye disease. Cell *141*, 178–190.